SI Appendix

Supplementary Information for

p53 prevents doxorubicin cardiotoxicity independent of its prototypical tumor suppressor activities

Jie Li[1]*, Ping-yuan Wang[1]*, Nathaniel A. Long[1], Jie Zhuang[1], Danielle A. Springer[2], Jizhong Zou[3], Yongshun Lin[3], Christopher K. E. Bleck[4], Ji-Hoon Park[1], Ju-Gyeong Kang[1], and Paul M. Hwang[1]

Author affiliation:
[1]Cardiovascular Branch, [2]Murine Phenotyping Core, [3]Induced Pluripotent Stem Cell Core, and [4]Electron Microscopy Core, National Heart, Lung, and Blood Institute, National Institutes of Health, Bethesda, Maryland, USA

*These authors contributed equally to this work.

Corresponding author:
Paul M. Hwang, MD, PhD
E-mail: hwangp@mail.nih.gov

This PDF file includes:
Supplementary text
SI Appendix, Figs. S1 to S11
References for SI

SI Materials and Methods

Mouse Cardiac Studies. Echocardiography was performed by an experienced cardiac sonographer without knowledge of mouse treatment status. Mice were lightly anesthetized with isoflurane, placed on a heated platform, and hair was removed with dilatory cream. ECG and rectal temperature were monitored during the studies. Parasternal long axis and mid-papillary short axis views of the left ventricle were acquired using the Vevo2100 ultrasound machine (VisualSonics) and a 30 MHz high frequency ultrasound probe (VisualSonics). LV systolic and diastolic wall thicknesses, and internal LV chamber dimensions were measured from 2-dimensional M-mode images. Ejection fraction and fractional shortening values were calculated through the system software.

Transmission Electron Microscopy (TEM). Mice were perfused with fixative solution (5% glutaraldehyde (EM Sciences) in 0.1 M sodium cacodylate buffer (pH 7.4)). The dissected tissues were post-fixed for 1 h (2.5% glutaraldehyde, 1% formaldehyde (EM Sciences) in 0.1 M sodium cacodylate buffer (pH 7.4)), additional post-fixation in 1% aqueous osmium tetroxide, block stained with 1% uranyl acetate, dehydrated in graded ethanol solutions, and embedded in EMbed-812 (EM Sciences). Thin sections were stained with uranyl acetate/lead citrate then examined on a JEM 1400 electron microscope (JEOL USA) with an bottom-mounted AMT XR-111 digital camera (Advanced Microscopy Techniques Corporation). The volume density and total surface area of cardiomyocyte mitochondria were quantified from TEM images using ImageJ software (Image Processing and Analysis in Java) and a previously described stereological technique (1, 2). This method uses 2-dimensional measurements to create 3-

dimensional data using geometric probability principles. The images were analyzed by two separate individuals without knowledge of sample identity.

TEM Stereological Measurements. Grids comprised of 0.5 μm or 1 μm squares were randomly overlaid on TEM images magnified 5,000x (0.5 μm scale bar) or 2,500x (2 μm scale bar), respectively. To extrapolate information from the TEM micrographs, a set of stereological equations was used as shown below (1). The volume fraction of mitochondria was calculated as the ratio of the volume of interest (Vi) to the total tested volume ($Vtest$), which is directly related to the ratio of the points of interest (Pi, white dots at the intersections of gridlines within the region of interest) to the total number of gridline intersection points ($Ptest$) (see equation and image below).

$$\frac{Vi}{Vtest} = \frac{Pi}{Ptest}$$

The surface area of the mitochondria was calculated as the ratio of the surface of interest (Si) per unit of total tested volume ($Vtest$) (see equation below). Ci corresponds to the points of intersection between the gridlines and the border of the region of interest (red dots around the mitochondria in the example image). $Ptest$ is as described above. d is the dimension (0.5 μm or 1 μm) of one gridline square.

$$\frac{Si}{Vtest} = \frac{Ci}{d \cdot Ptest}$$

Antibodies. Antibodies utilized in this study were as follows: α-actinin mouse monoclonal antibody (mAb, A7811) (Sigma-Aldrich); ATP5A mouse mAb (sc-136178), MT-ND4 rabbit polyclonal antibody (pAb, sc-20499), p53 mouse mAb (DO1, sc-126) (Santa Cruz Biotech. Inc.); MT-ATP6 rabbit pAb (55313-1-AP) (Proteintech); Bax rabbit pAb (2772) , Cleaved Caspase-3

rabbit mAb (#9664), Cleaved PARP rabbit pAb (9544); BNIP3 rabbit pAb (3769) (Cell Signaling Technology); MT-CO1 mouse mAb (ab14705), COX4 rabbit pAb (ab16056), human p53R2 rabbit pAb (ab8105), mouse TFAM rabbit pAb (ab131607), human TFAM rabbit pAb (ab47517), TOP2B rabbit pAb (ab109524) (Abcam); cardiac troponin T mouse mAb (CTNT) (CT3, Developmental Studies HybridomaBank, http://dshb.biology.uiowa.edu); MT-CYB rabbit pAb (LS-C411296) (LSBio); GAPDH mouse mAb (AM4300), (Thermo Fisher Scientific); NDUFA9 mouse mAb (A21344), NQCRFS1 mouse mAb (A21346), SDHA mouse mAb (A11142), SDHB mouse mAb (A21345) (Molecular Probe); human p21 mouse mAb (OP64, Calbiochem); TOP1MT rabbit pAb (ARP66489_P050) (Aviva Systems Biology).

Confocal Immunofluorescence Microscopy. Differentiation of human iPS cells into cardiomyocytes was confirmed by immunofluorescence as previously described (3). Briefly, iPSCs or cardiomyocytes were fixed with 2% paraformaldehyde/PBS at 21 ºC for 10 min, permeabilized with 0.2% Triton X-100/PBS for 3 min, blocked with 10 mg/ml BSA for 30 min, incubated with α-actinin, cardiac troponin T, SOX2, NKX2.5 or Ki67 antibody (Life Technologies) at 4 °C overnight, followed by Alexa Fluor 488-labeled secondary antibody (Invitrogen) at 21 °C for 1 hr. Cell nuclei were stained with DAPI (Invitrogen) and visualized using a confocal laser-scanning microscope (Zeiss LSM 880).

TUNEL Assay. Apoptosis in paraffin-embedded tissue sections (10 μm) were detected by using the terminal deoxynucleotidyl transferase–mediated dUTP-digoxigenin nick-end labeling (TUNEL) assay and quantified as previously described (4).

List of PCR Primer Sequences.

PCR primers for mtDNA copy number:

Human and mouse 18sRNA
F 5'-CTTAGAGGGACAAGTGGCGTTC
R 5'-CGCTGAGCCAGTCAGTGTAG

Human MT-CO2
F 5'-CAGACGAGGTCAACGATCCCTC
R 5'-GCATGAAACTGTGGTTTGCTCCACAG

Mouse MT-CO2
F 5'-CCATAGGGCACCAATGATACTG
R 5'-AGTCGGCCTGGGATGGCATC

PCR primers for mtDNA integrity:

Mouse:

Long fragment
F 5'-GCCAGCCTGACCCATAGCCATATTAT
R 5'-GAGAGATTTTATGGGTGTATTGCGG

Short fragment
F 5'-CCCAGCTACTACCATCATTCAAGT
R 5'-GATGGTTTGGGAGATTGGTTGATG

Human:

Long fragment
F 5'-TGAGGCCAAATATCATTCTGAGGGGC
R 5'-TTTCATCATGCGGAGATGTTGGATGG

Short fragment
F 5'-CCCCACAAACCCCATTACTAAACCCA
R 5'-TTTCATCATGCGGAGATGTTGGATGG (same as for long fragment)

PCR primers for mRNA quantification:

Human:

MT-ATP6
F 5'-CGCCACCCTAGCAATATCAA
R 5'-TTAAGGCGACAGCGATTTCT

MT-ATP8
F 5'-CCCTCACCAAAGCCCATAAA
R 5'-GGCAATGAATGAAGCGAACAG

MT-CO1
F 5’-CTTCGTCTGATCCGTCCTAATC
R 5’-TTGAGGTTGCGGTCTGTTAG

MT-CO2
F 5’-CAGCGCAAGTAGGTCTACAA
R 5’-CATACAGGACTAGGAAGCAGATAAG

MT-CO3
F 5’-CGAGTCTCCCTTCACCATTTC
R 5’-TTGGCGGATGAAGCAGATAG

MT-CYB
F 5’-GCGTCCTTGCCCTATTACTATC
R 5’-CTGCGGCTAGGAGTCAATAAA

MT-ND1
F 5’-CACCCTCACCACTACAATCTTC
R 5’-GGGAGGTTAGAAGTAGGGTCTT

MT-ND2
F 5’-ACCGTACAACCCTAACATAACC
R 5’-TCGTGGTGCTGGAGTTTAAG

MT-ND3
F 5’-CTACCATGAGCCCTACAAACA
R 5’-GTCACTCATAGGCCAGACTTAG

MT-ND4
F 5’-CTCTCACTGCCCAAGAACTATC
R 5’-GGGCTTTAGGGAGTCATAAGTG

MT-ND4L
F 5’-CACACCTCATATCCTCCCTACT
R 5’-TAAGAGGGAGTGGGTGTTGA

MT-ND5
F 5’-AACACTATGCTTAGGCGCTATC
R 5’-AACACTATGCTTAGGCGCTATC

MT-ND6
F 5’-GTTTCTGTTGAGTGTGGGTTTAG
R 5’-CCACACCGCTAACAATCAATAC

MT-RNR1

F 5’-TCTAGAGGAGCCTGTTCTGTAA
R 5’-TGTAGCCTTCATCAGGGTTTG

MT-RNR2
F 5’-GGGTTCAGCTGTCTCTTACTTT
R 5’-TCCATAGGGTCTTCTCGTCTT

p21
F 5’-CCCGTCTCAGTGTTGAGCCTT
R 5’-GTTCCGCTGCTAATCAAAGTGC

TFAM
F 5’-ATAGGCACAGGAAACCAGTTAG
R 5’-GCAGAAGTCCATGAGCTGAATA

Mouse:

MT-ATP6
F 5’-CCACCAACAGCTACCATTACA
R 5’-AGGCTTACTAGGAGGGTGAATA

MT-ATP8
F 5’-TGCCACAACTAGATACATCAACA
R 5’-AGTGGGAATGTTTGTGATGAGA

MT-CO1
F 5’-CCAGATATAGCATTCCCACGAATA
R 5’-CCTGCTCCTGCTTCTACTATTG

MT-CO2
F 5’-AGGGCACCAATGATACTGAAG
R 5’-CAGTCGTAGTTCACCAGGTTT

MT-CO3
F 5’-TTTCAGCCCTCCTTCTAACATC
R 5’-GTGAGTAGGCCAAGGGTTAATAG

MT-CYB
F 5’-CATGTCGGACGAGGCTTATATT
R 5’-GCTATGACTGCGAACAGTAGAA

MT-ND1
F 5’-CAATTTACCAGAACTCTACTCAACTAAC
R 5’-CGTAACGGAAGCGTGGATAA

MT-ND2
F 5’-TGAGGAGGACTTAACCAAACAC

R 5’-GGGATGGGTTGTAAGGAAGAAT

MT-ND3
F 5’-CTCTGCACGTCTACCATTCTC
R 5’-GCTCATGGTAGTGGAAGTAGAAG

MT-ND4
F 5’-GAACCAAACTGAACGCCTAAAC
R 5’-GAGGGCAATTAGCAGTGGAATA

MT-ND4L
F 5’-CCACATTACTATGCCTGGAAGG
R 5’-GGGATTGGTATGGAGCTTATGG

MT-ND5
F 5’-CGGAGCCCTAACCACATTATT
R 5’-GCCTAGTTGGCTTGATGTAGAG

MT-ND6
F 5’-GTTTGGGAGATTGGTTGATGTATG
R 5’-CACCCAGCTACTACCATCATTC

MT-RNR1
F 5’-GGTTTGGTCCTGGCCTTAT
R 5’-GTGCTTGATACCCTCTCCTTAAA

MT-RNR2
F 5’-GCCCTAGCCCTACACAAATATAA
R 5’-CATCTTTCCCTTGCGGTACT

p21
F 5’-AGGGCAACTTCGTCTGGGAG
R 5’-TTGGAGACTGGGAGAGGGCA

TFAM
F 5’-CTGATGGGTATGGAGAAGGAGG
R 5’-CCAACTTCAGCCATCTGCTCTTC

PCR primers for Chip assay:

ETS2-binding region in *TFAM*
F 5’- GCATGATAACACACGCCGGAG
R 5’- CACATGCTTCGGAGAAACGCCATC

p53-binding motif in *p21*
F 5’- CCATCCCTATGCTGCCTGCTTC

R 5’- GCTGGCAGATCACATACCCTG

ETS2-binding region in *MLL1*
F 5’- GGCATGCAGTTATCCAGGTTGC
R 5’- GGCCTCCGCCTCTGACGCCTGG

Non-specific (NS) control *B2M*
F 5’-GCTGGGTAGCTCTAAACAATGTATTCA
R 5’- CCATGTACTAACAAATGTCTAAAATGGT

References

1. Mobley BA & Eisenberg BR (1975) Sizes of components in frog skeletal muscle measured by methods of stereology. *J Gen Physiol* 66(1):31-45.
2. Wu HD*, et al.* (2012) Ultrastructural remodelling of Ca(2+) signalling apparatus in failing heart cells. *Cardiovasc Res* 95(4):430-438.
3. Lin Y*, et al.* (2017) Heparin Promotes Cardiac Differentiation of Human Pluripotent Stem Cells in Chemically Defined Albumin-Free Medium, Enabling Consistent Manufacture of Cardiomyocytes. *Stem Cells Transl Med* 6(2):527-538.
4. Park JH*, et al.* (2018) Mouse Homolog of the Human TP53 R337H Mutation Reveals Its Role in Tumorigenesis. *Cancer Res* 78(18):5375-5383.

Fig. S1

A

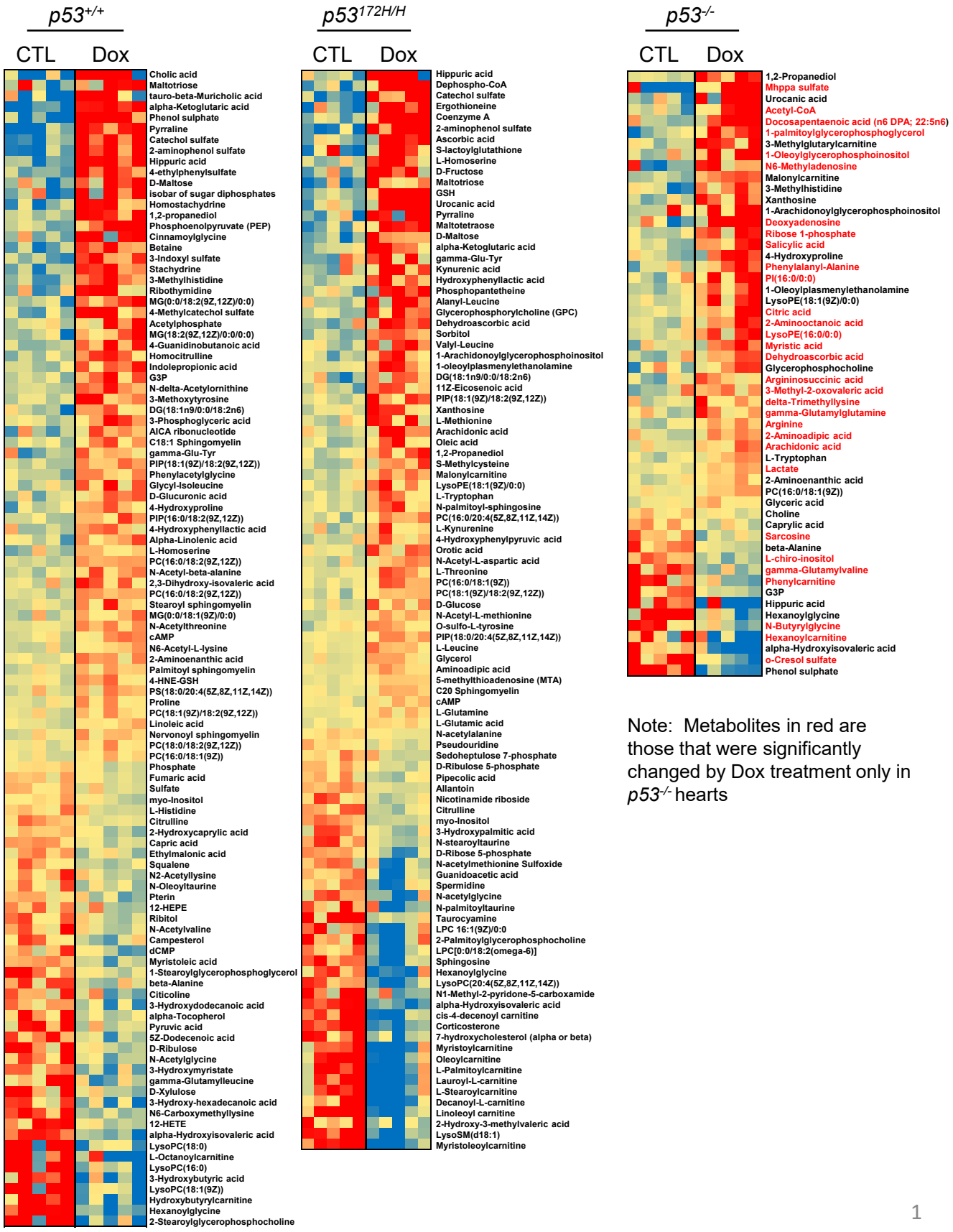

Note: Metabolites in red are those that were significantly changed by Dox treatment only in *p53*$^{-/-}$ hearts

B

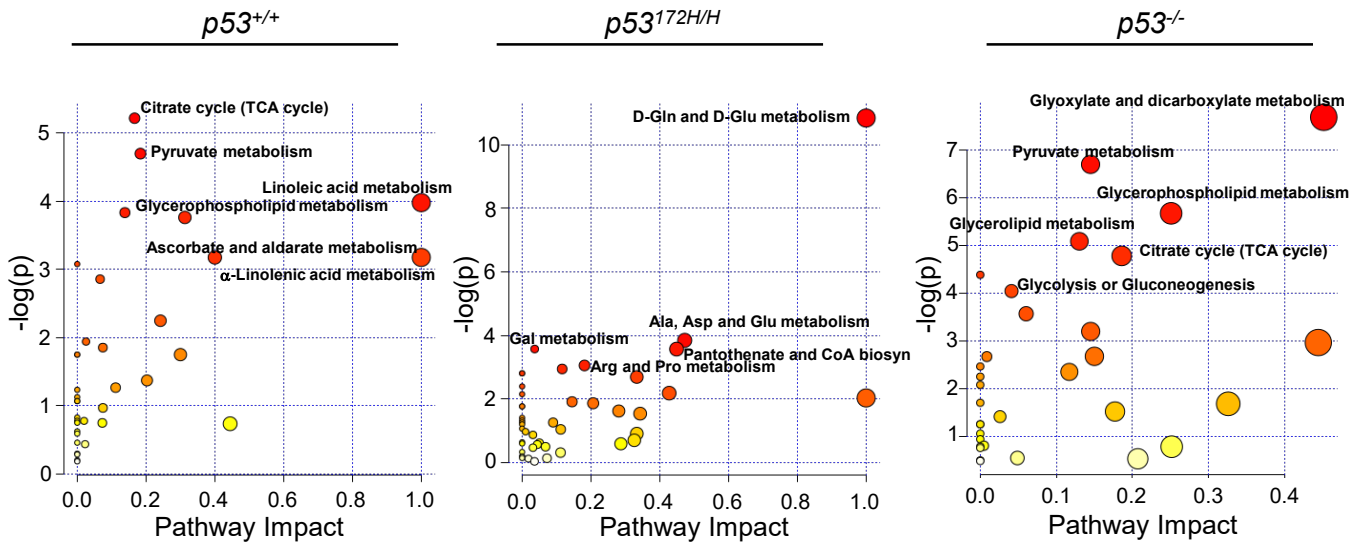

Fig. S1. Distinct metabolomic changes are induced by Dox treatment in p53 null hearts while mutant p53 samples display partial overlap with wild-type and null states. (**A)** Heat map of metabolites significantly affected in hearts of mice treated with divided low doses of Dox per protocol compared with untreated controls (CTL) of the indicated *p53* genotype at study week 10 (n = 5). Metabolite ion abundance was normalized to the median and log2 transformed. Normalized ion abundance is color coded in the range of +0.7 (Red) to -1.5 (Blue). (**B)** MetaboAnalyst software (v3.0, McGill University) was used to identify metabolic pathways that were differentially affected by Dox treatment. The size and color of each circle represent pathway impact and *P*-value, respectively. Significantly and highly impacted pathways are labeled. Statistical testing in **(A)** by 2-way ANOVA in comparison with untreated control of corresponding *p53* genotype, considered significant if $P < 0.05$.

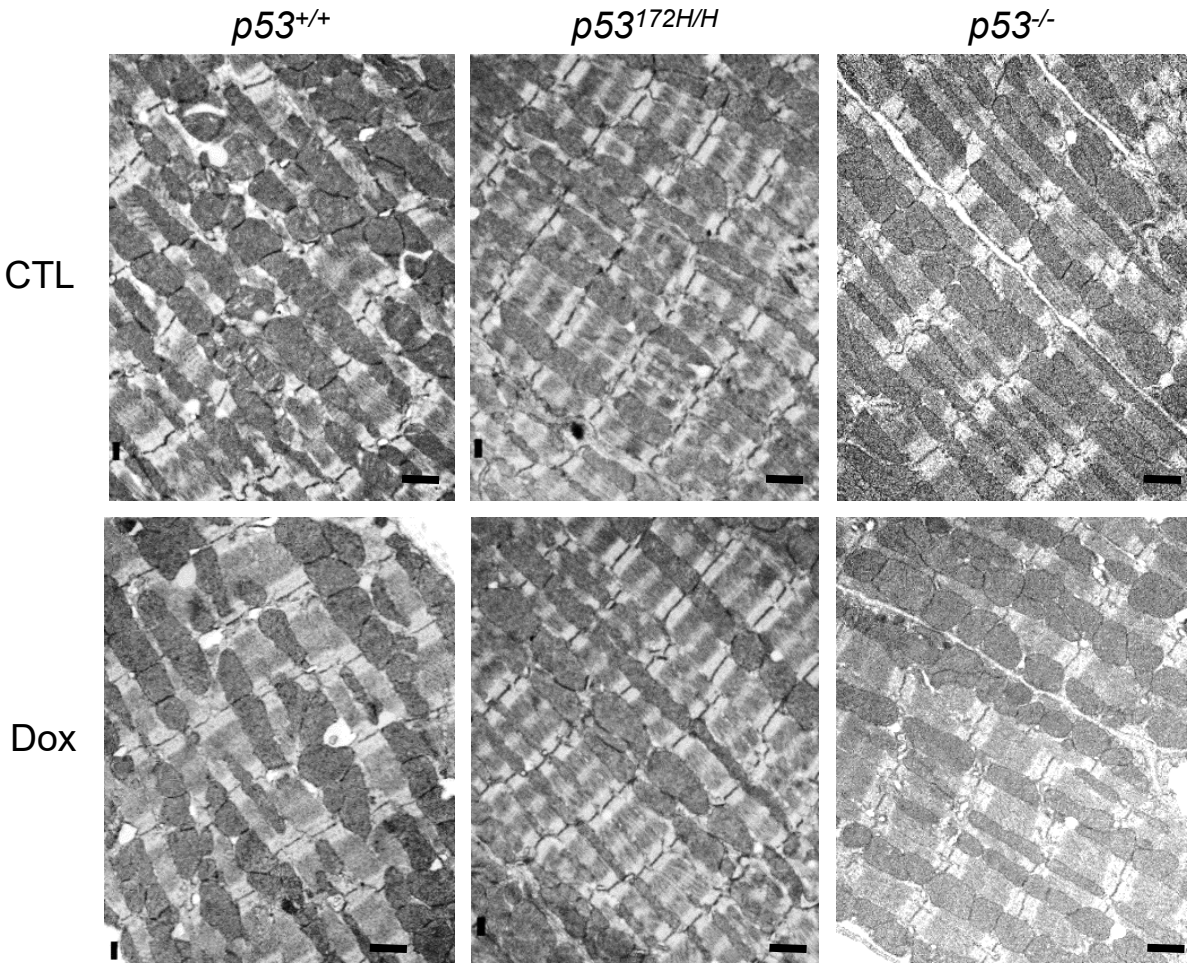

Fig S2, Representative TEM images of control (CTL) and Dox-treated mouse hearts at the end of study week 10. Scale bar = 1 μm.

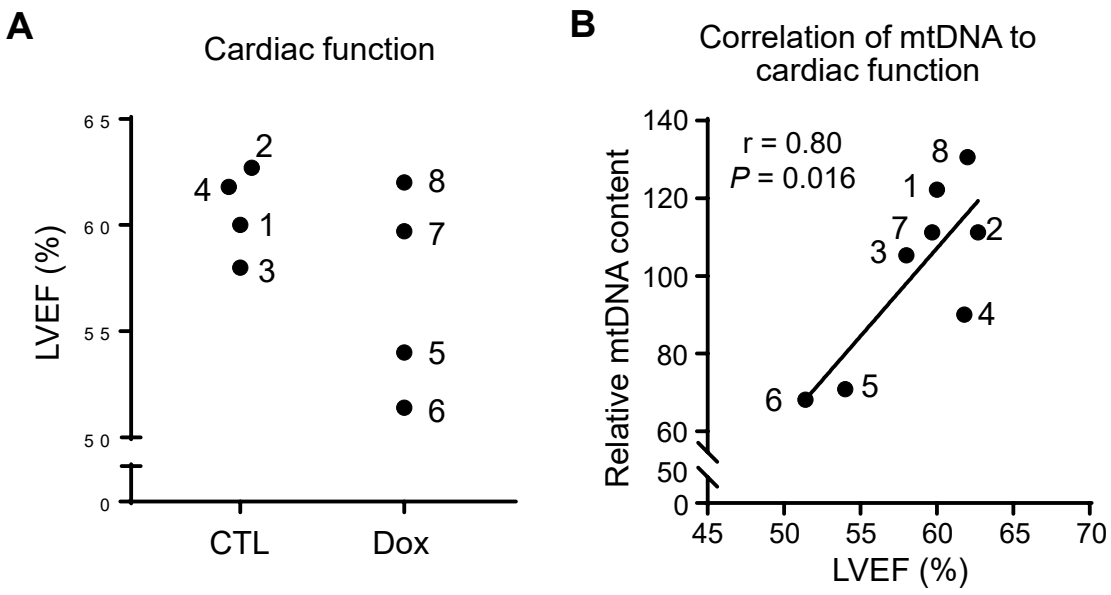

Fig. S3. Long-term effect of doxorubicin treatment on wild-type mouse hearts. *p53*$^{+/+}$ mice (~4 wk old) were treated with divided low doses of Dox and analyzed ~80 wk after treatment. (**A)** Left ventricular ejection fraction (LVEF%) was measure in untreated control (CTL) and Dox treated mice by echocardiography. Individual mice are represented by unique numbers. (**B)** Correlation of cardiac mtDNA content with LVEF by Pearson correlation coefficient test.

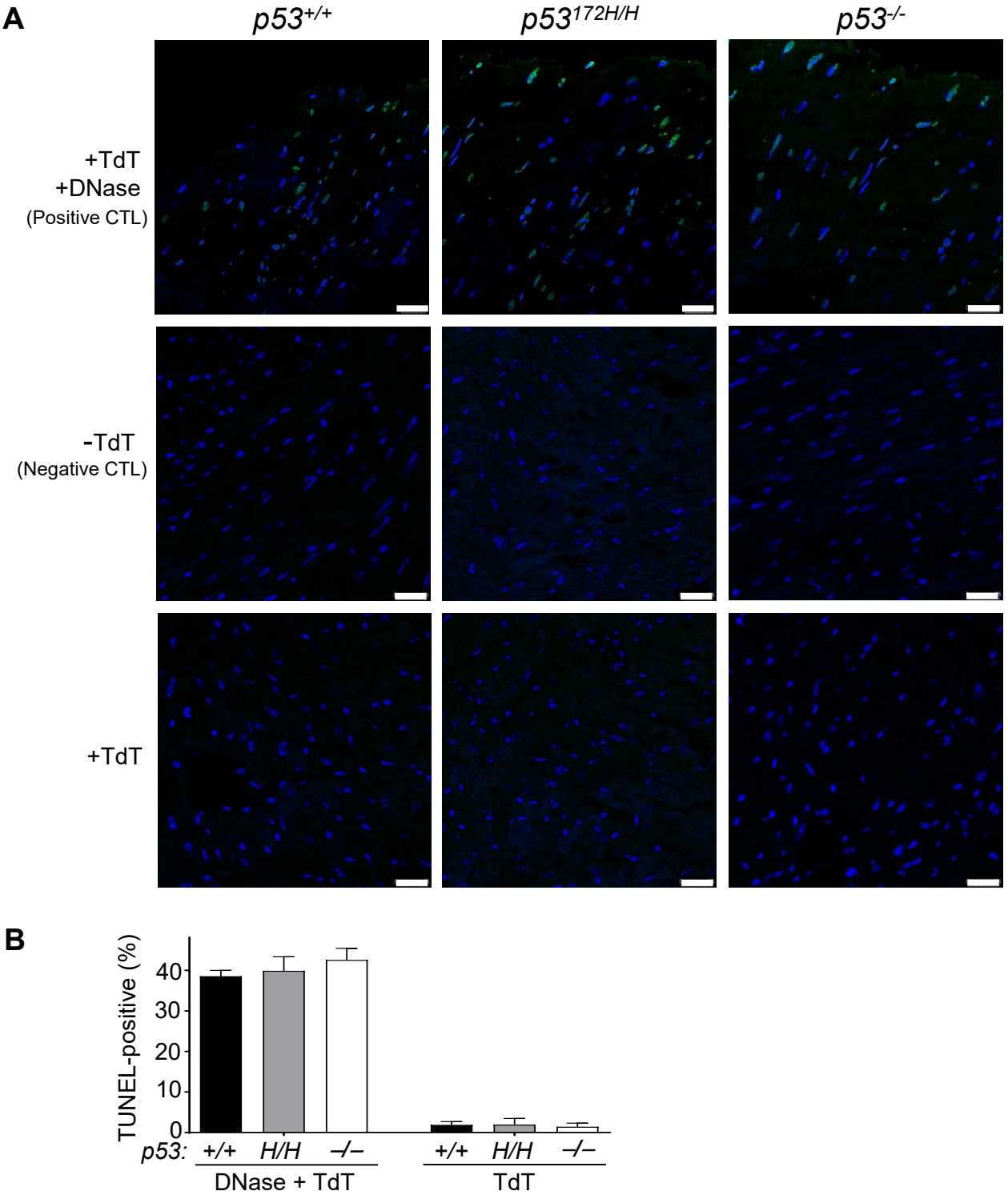

Fig. S4. TUNEL staining for apoptosis in the hearts of mice treated with low dose Dox. (A) Representative images of TUNEL stained heart tissue sections collected at study week 10 per treatment protocol. Top row, positive control (CTL) with addition of terminal deoxynucleotidyl transferase (+TdT) and DNase. Note scattered TUNEL-positive green fluorescence in all 3 genotypes of *p53*. Middle row, negative control without TdT. Bottom row, addition of TdT does not reveal significant TUNEL staining in any of the *p53* genotypes. Blue DAPI signals indicate nuclear staining. Scale bar = 25 μm. (B) Quantification of TUNEL-positive nuclei (n ≥ 5-7). DNase samples serve as positive control.

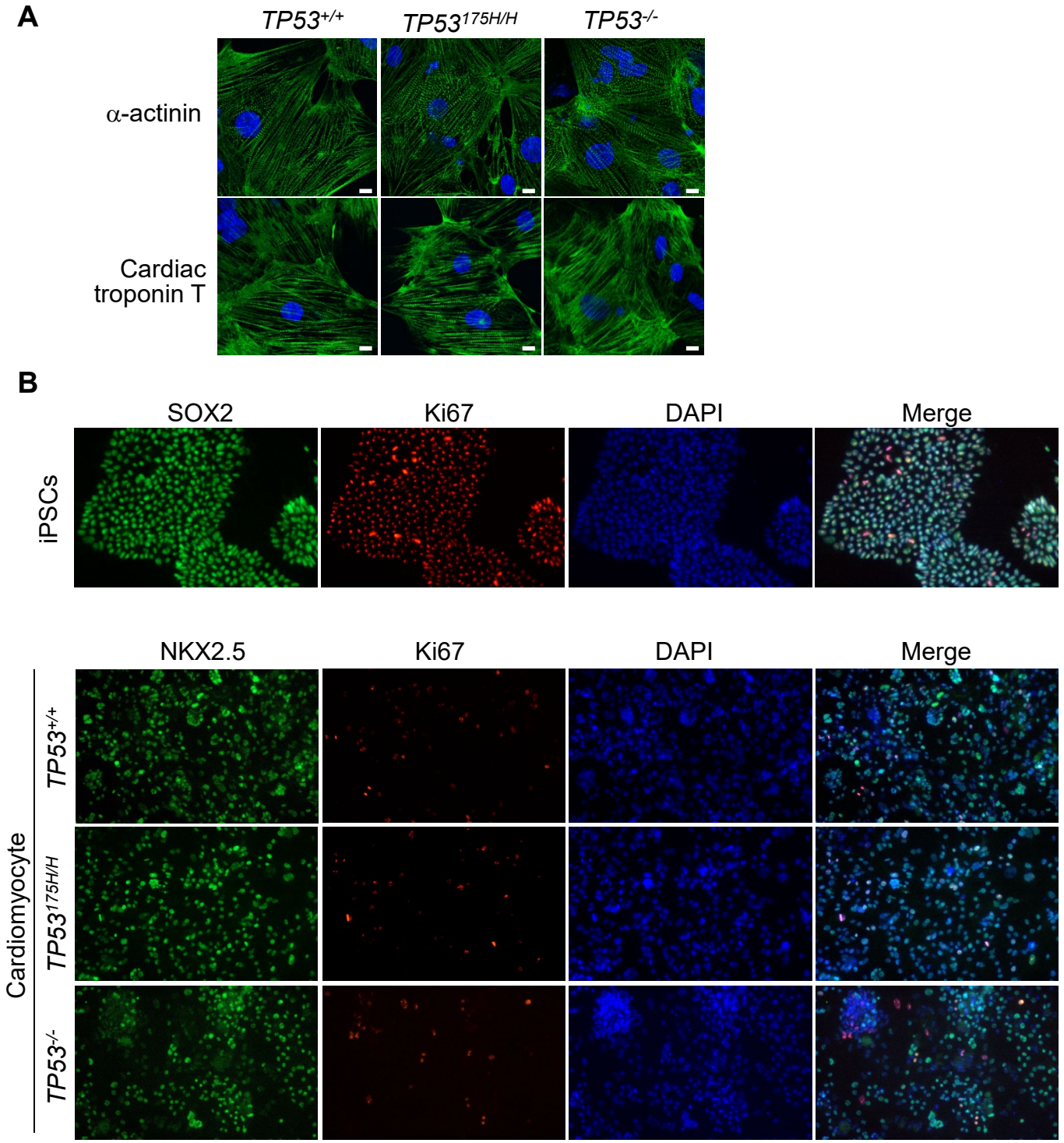

Fig. S5. Characterization of day 30 cardiomyocytes differentiated from human *TP53*$^{+/+}$, *TP53*$^{175H/H}$ and *TP53*$^{-/-}$ iPS cells. (A) α-actinin or cardiac troponin T antibody staining (green) of the iPSC-derived cardiomyocytes. Scale bar = 10 μm. (B) Upper panel: iPSCs (*TP53*$^{+/+}$) were stained with stem cell marker SOX2 and Ki67 as marker of proliferation. Lower panel: cardiomyocytes were stained with cardiac lineage marker NKX2.5 and Ki67 as marker of proliferation. The percentages of Ki67-positive *TP53*$^{+/+}$, *TP53*$^{175H/H}$ and *TP53*$^{-/-}$ cardiomyocytes were 5.8 ± 0.3, 5.7 ± 0.6, and 7.1 ± 1.7 (mean ± SD), respectively (*P* = *NS*, n=3). DAPI blue fluorescence signals indicate DNA staining of nuclei.

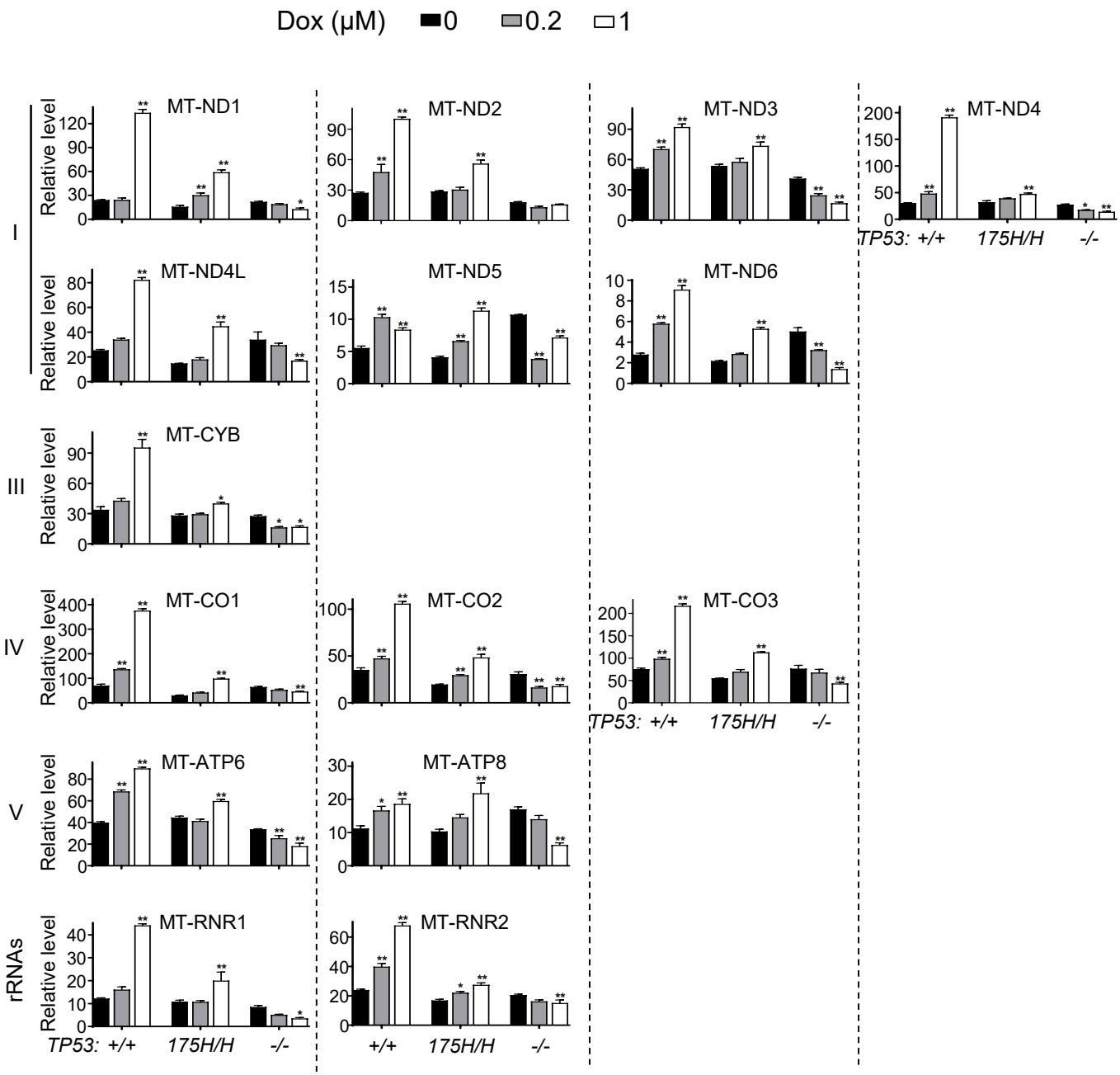

Fig. S6. Individual mtDNA-encoded mitochondrial transcripts are downregulated in *TP53*$^{-/-}$ cardiomyocyte by doxorubicin treatment while being upregulated in both *TP53*$^{+/+}$ and *TP53*$^{175H/H}$ cardiomyocytes. Human iPSC-derived cardiomyocytes were treated with the indicated concentrations of Dox for 48 h before quantification of mtDNA-encoded mitochondrial respiratory complex subunit (grouped by complexes I-V) and rRNA gene expression by real time RT-PCR (n ≥ 3). Statistical testing by 2-way ANOVA in comparison with corresponding genotype untreated control. Values are mean ± SEM, **P* < 0.05; ***P* < 0.01.

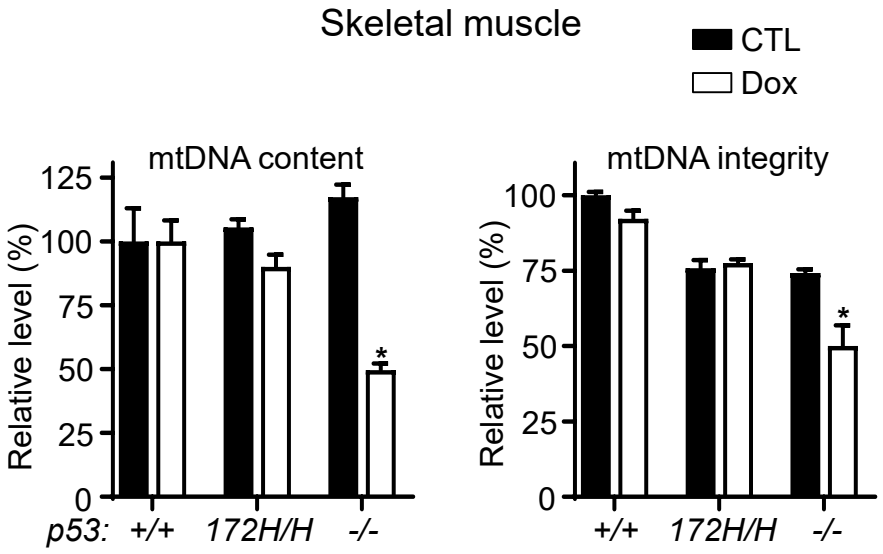

Fig. S7. Analysis of mtDNA in mouse skeletal muscle by *p53* genotype. mtDNA content and integrity in soleus skeletal muscle at study week 10 after low dose Dox treatment (n ≥ 3). Statistical testing by 2-way ANOVA in comparison with corresponding untreated control. Values are mean ± SEM, **P* < 0.05.

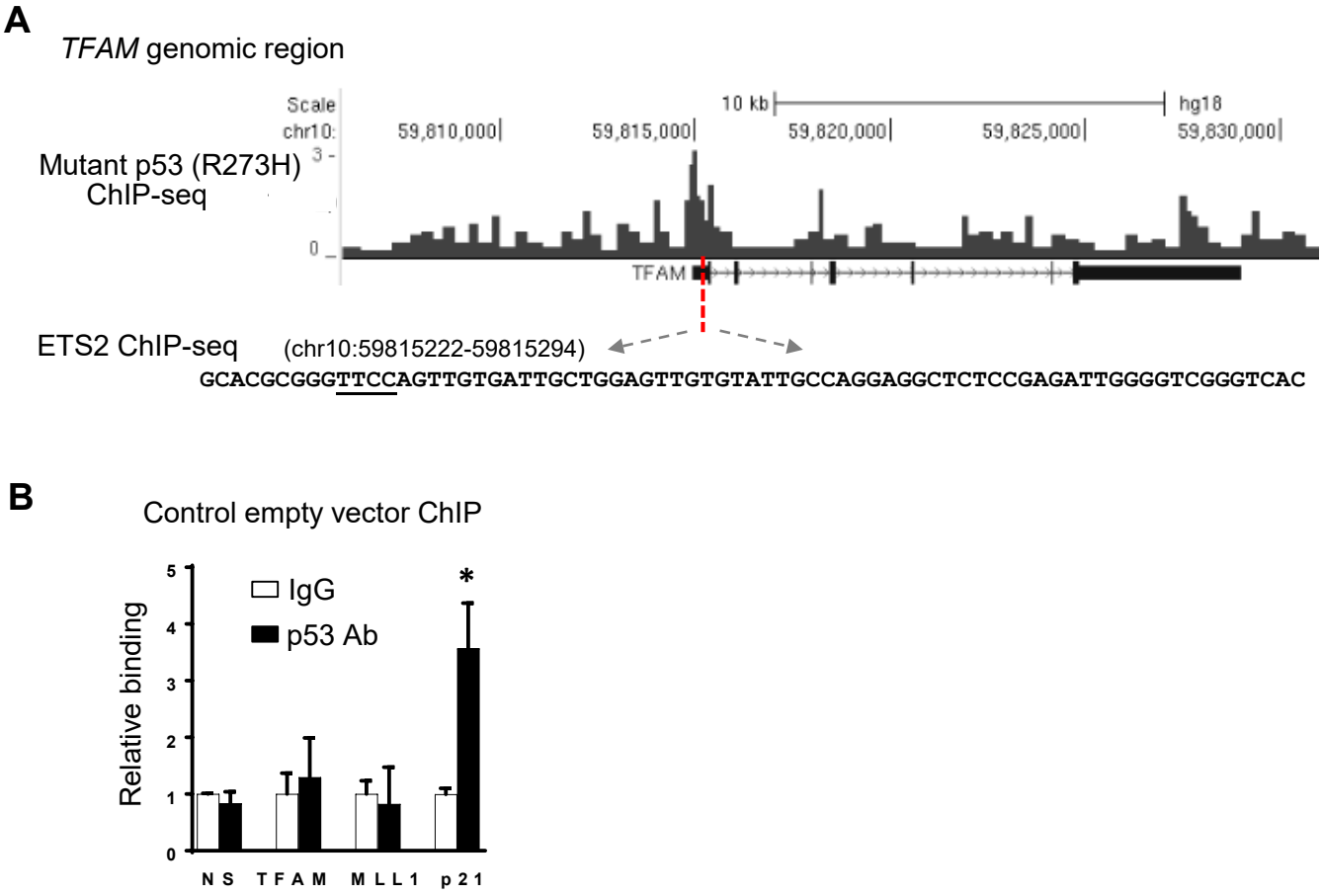

Fig. S8. Identification of a ETS2 motif in *TFAM* gene that interacts with a mutant of p53, and negative control for p53 ChIP assay. (A) Analysis of previously published wild-type and mutant R273H p53 ChIP-seq and ETS2 ChIP-seq databases identifies a mutant p53 interacting ETS2–binding sequence motif in exon 1 of *TFAM* (red dashed line with expanded sequence). Shown is the ChIP-seq profile/peaks of mutant p53 binding across the *TFAM* gene locus. (**B)** p53 ChIP of human myoblasts transduced with empty vector lentivirus as a control for Fig. 5B. p53 binding is shown relative to nonspecific IgG samples. Note that it shows only endogenous wild-type p53 binding to the p53-response element of *p21* (*CDKN1A*) as a positive control. Statistical testing by unpaired *t* test in comparison with IgG control. Values are mean ± SEM, **P* < 0.05

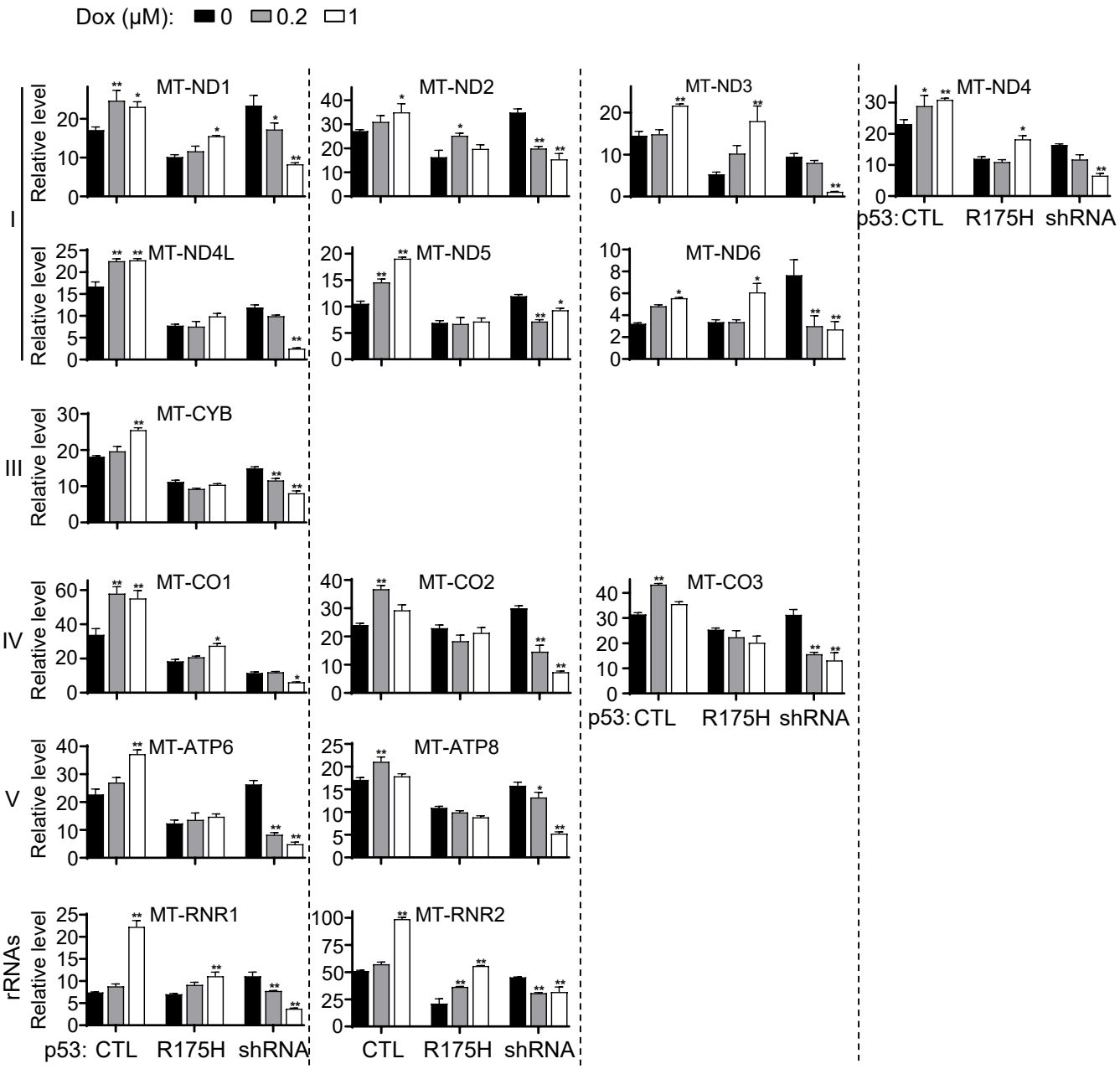

Fig. S9. Knocking down p53 in human skeletal muscle myoblasts results in inhibition of mtDNA transcription by doxorubicin. Human myoblasts with wild-type p53 were transduced with control lentivirus or lentivirus expressing mutant human p53 R175H or shRNA to knockdown endogenous p53. Cells were treated with the indicated concentrations of Dox for 16 h and individual mtDNA-encoded RNAs (grouped by respiratory complexes I-V) were quantified by real time RT-PCR (n ≥ 3). Statistical testing by 2-way ANOVA with corresponding group untreated control. Values are mean ± SEM, **P* < 0.05; ***P* < 0.01.

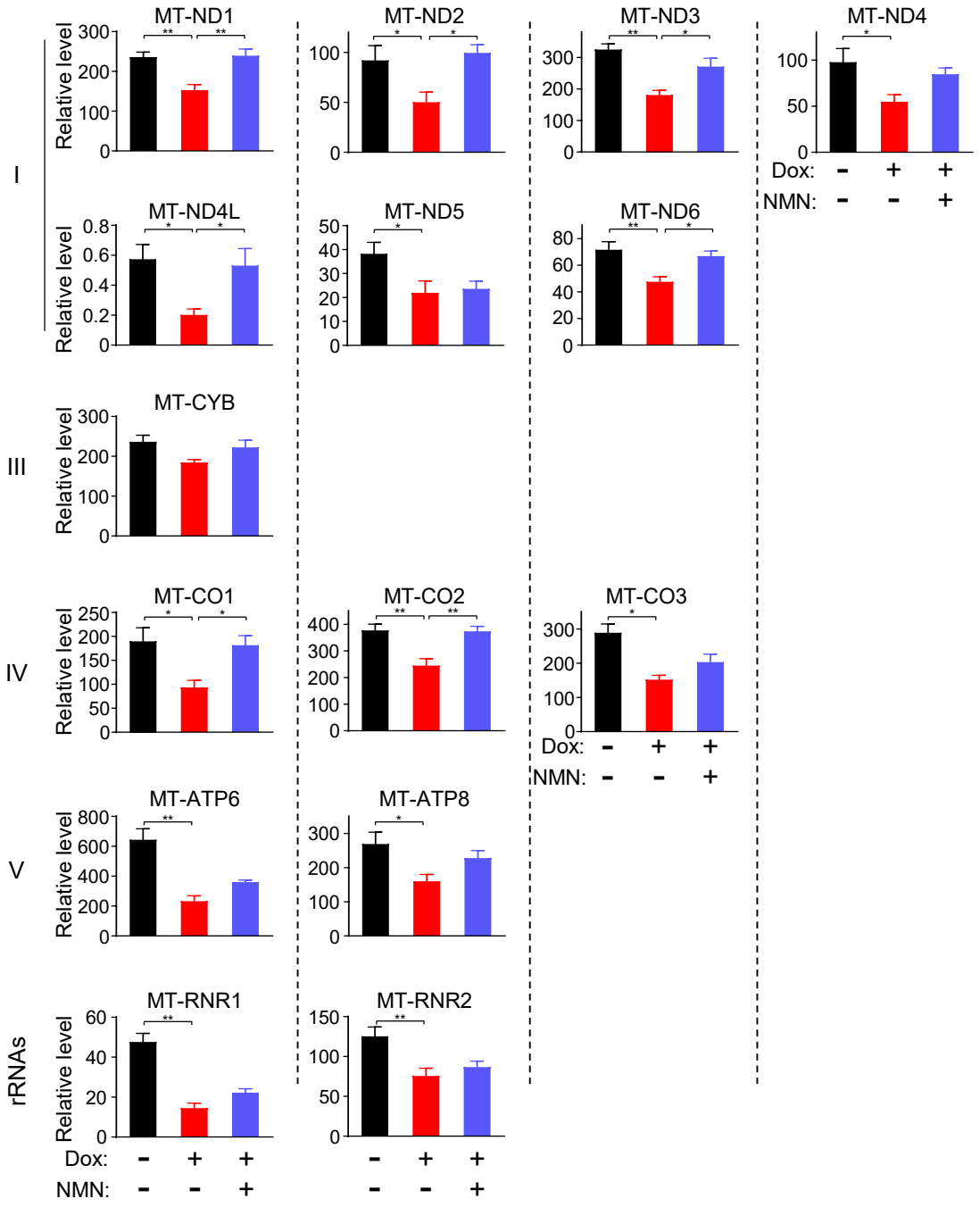

Fig. S10. Nicotinamide mononucleotide rescues the inhibition of mtDNA transcription by doxorubicin in *p53*$^{-/-}$ mice. *p53*$^{-/-}$ mice were treated with divided low doses of Dox per protocol and with either vehicle control or NMN i.p. (3 times per wk) over the duration of the entire study. Individual mtDNA-encoded RNAs (grouped by respiratory complexes I-V) in cardiac tissue were quantified by real time RT-PCR (n = 8). Statistical testing by 1-way ANOVA between indicated samples. Values are mean ± SEM, **P* < 0.05; ***P* < 0.01.

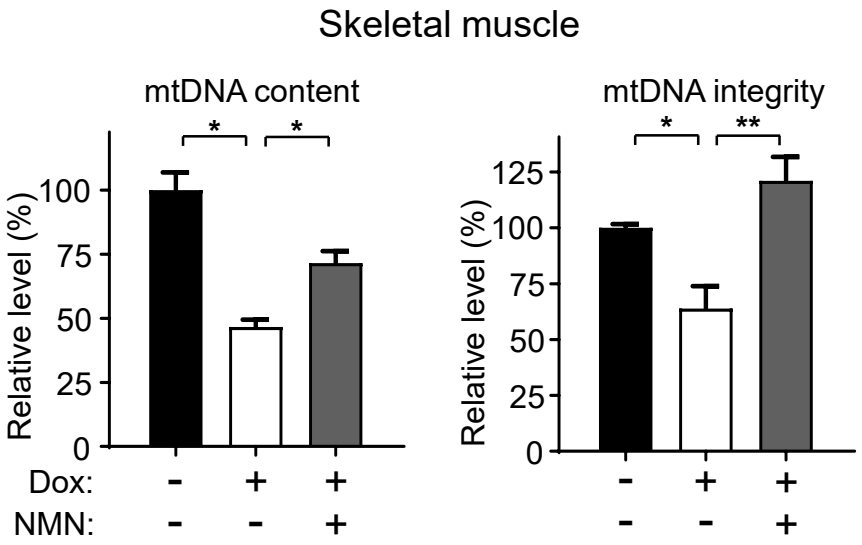

Fig. S11. NMN treatment prevents mtDNA damage and depletion by Dox in skeletal muscle of *p53*$^{-/-}$ mice. *p53*$^{-/-}$ mice were treated with divided low doses of Dox per protocol and with either vehicle control or NMN i.p. (3 times per wk) over the entire duration of the study. mtDNA content and integrity of soleus skeletal muscle were quantified at study week 10 (n ≥ 3). Statistical testing by 1-way ANOVA between indicated samples. Values are mean ± SEM, **P* < 0.05; ***P* < 0.01.